Geoelectrical signatures of reactive mixing: a theoretical assessment

Uddipta Ghosh, Tanguy Le Borgne, D. Jougnot, Niklas Linde, Yves Méheust

AGU PUBLICATIONS

Geophysical Research Letters

RESEARCH LETTER
10.1002/2017GL076445

Key Points:
- We propose a new approach for geoelectrical monitoring of mixing processes by exploring electrically sensitive reactions in mixing fronts
- Effective conductivity is highly sensitive to reactive mixing; its anisotropy depends on velocity, reaction kinetics, and front orientation
- This article can be an important stepping stone for developing noninvasive tools to monitor reactive mixing in the subsurface

Supporting Information:
- Supporting Information S1

Correspondence to:
U. Ghosh,
uddiptakgp@gmail.com

Citation:
Ghosh, U., Borgne, T. L., Jougnot, D., Linde, N., & Méheust, Y. (2018). Geoelectrical signatures of reactive mixing: A theoretical assessment. *Geophysical Research Letters*, *45*, 3489–3498. https://doi.org/10.1002/2017GL076445

Received 17 NOV 2017
Accepted 21 FEB 2018
Accepted article online 27 FEB 2018
Published online 16 APR 2018

Geoelectrical Signatures of Reactive Mixing: A Theoretical Assessment

U. Ghosh[1,2], T. L. Borgne[1], D. Jougnot[3], N. Linde[4], and Y. Méheust[1]

[1]Université de Rennes 1, CNRS, Géosciences Rennes UMR6118, Rennes, France, [2]Department of Mechanical Engineering, Indian Institute of Technology Gandhinagar, Gandhinagar, India, [3]Sorbonne Universités, UPMC Univ. Paris 06, CNRS, EPHE, UMR 7619 METIS, Paris, France, [4]Applied and Environmental Geophysics Group, Institute of Earth Sciences, University of Lausanne, Lausanne, Switzerland

Abstract Characterizing the effects of subsurface fluid mixing on biogeochemical reactions is a key step toward monitoring and understanding a range of processes and applications in which fluids of different chemical compositions mix, such as aquifer remediation, CO_2 sequestration, or groundwater-surface water interactions. Yet the development of noninvasive methods to monitor mixing processes remains an outstanding challenge. Mixing processes are controlled by concentration gradients that develop at scales below the spatial resolution of hydrogeophysical imaging techniques. To overcome this difficulty, we propose to focus on the geoelectrical response of mixing-driven chemical reactions, for which the products are electrically more conductive than the background solution. For such reactions, we investigate the impact of reactive mixing on the resulting effective electrical conductivity. The transport equations are solved using the Lamellar Mixing Theory for a range of velocity gradients representative of the stretching rates experienced by mixing fronts in heterogeneous porous media. Focusing on simple shear flows, we demonstrate that such reactions may result in substantial changes (several orders of magnitude) in the effective conductivity over time, thus providing geoelectrical signatures of reactive mixing dynamics. The temporal evolution of the effective conductivity depends on the relative orientations of the applied electrical potential gradient, mean flow, and velocity gradient, yielding different sensitivities to dispersion processes, stretching rates, and reaction kinetics. These results suggest that the use of chemical reactions with electrically conductive products could help to overcome present limitations of time-lapse geophysical imaging in the monitoring of the spatiotemporal dynamics of subsurface reactive mixing processes.

Plain Language Summary It is a well-known fact that mixing of fluids with different chemical compositions in the subsurface plays a key role in various biological and geochemical reactions. The simplest way to gain insight into any reaction is to have an accurate estimate of the mass of the products(s) and its distribution. When such reactions are accompanied by fluid flow, additional complexities arise because the flow sweeps away the reactants in different directions, leading to mixing and spreading. Since the flow in the subsurface is intricate, this creates complex mixing and reaction patterns. In addition to this, the opacity of the subsurface prevents us from having easy access to these reactions, which poses serious difficulties in properly monitoring the subsurface reactive mixing processes. In the present work, we show that it might be possible to indirectly monitor the state of the some special kinds of reactions by measuring the electrical conductivity of the subsurface. In more technical terms, here we show that for reactions generating products with significantly different electrical conductivities as compared to the reactants, the effective conductivity is intricately linked to the reaction rate, the mixing rate, and the geometry of the reaction hot spots.

1. Introduction

In subsurface hydrology, mixing processes occurring at interfaces between fluids of different chemical compositions play a key role in controlling the effective dilution rates of dissolved chemical species, as well as fluid-fluid and fluid-mineral reaction rates (Cil et al., 2017; De Simoni et al., 2005; Dentz et al., 2011; Rolle et al., 2009). Mixing interfaces, which are naturally present in coastal aquifers and hyporheic zones beneath rivers, are thus known to be reactive hot spots for biogeochemical processes (Appelo & Postma, 2004; Boano et al., 2014; McClain et al., 2003). Mixing fronts are also created when injecting fluids in the subsurface,

such as in CO_2 sequestration, geothermal doublets, aquifer remediation, or artificial recharge operations, which leads to a range of biogeochemical reactions that may affect the feasibility and sustainability of these activities (Hidalgo et al., 2015; Kitanidis & McCarty, 2012; Possemiers et al., 2016). The development of relevant mixing models has led to significant advances in the quantification of mixing rates (Chiogna et al., 2012; Cirpka & Kitanidis, 2000; Kitanidis, 1994; Le Borgne et al., 2010), how to relate them to medium heterogeneity at different scales (de Barros et al., 2012; Le Borgne et al., 2015, 2013; Lester et al., 2013; Ye et al., 2015) and how to predict their impact on biogeochemical reaction rates (Bandopadhyay et al., 2017; Cirpka et al., 2008; de Anna, Dentz, et al., 2014; de Anna, Jimenez-Martinez, et al., 2014; Engdahl et al., 2014; Le Borgne et al., 2014; Luo et al., 2008). Despite the progress in our understanding of reaction kinetics subject to mixing in heterogeneous media, quantitative monitoring of such processes in the field remains an outstanding challenge.

The primary sources of difficulties in monitoring subsurface processes is related to the opacity of the medium, its heterogeneity, and poor spatial coverage when only using data acquired within or in the immediate vicinity of boreholes. Time-lapse (i.e., repeated) geophysical imaging makes it possible to noninvasively and remotely track the motion and spatial distributions of tracers using surface- or borehole-based sensor deployments (e.g., Binley et al., 2015; Dorn et al., 2011; Hubbard & Linde, 2011). In this respect, time-lapse electrical resistivity tomography (Daily et al., 1992) has been widely used in conjunction with saline tracers to map flow paths and related processes (Cassiani et al., 2006). Another suitable electrical method is spectral induced polarization measurements (Binley et al., 2015; Kemna et al., 2012). Furthermore, the developing field of biogeophysics has demonstrated geophysical signatures related to biogeochemical processes and products (Atekwana & Slater, 2009; Knight et al., 2010). Many time-lapse geophysical studies have focused on dispersion and biogeochemical processes, but they have not yet addressed in situ characterization of mixing processes. Deterministic reconstruction of concentration fields from geophysical methods offers insufficient resolution to predict mixing (Binley et al., 2002; Briggs et al., 2013, 2014; Day-Lewis et al., 2017; Doetsch et al., 2012; Jougnot et al., 2018; Singha & Gorelick, 2005). Hence, mixing rates estimated from such reconstructed concentration fields would be inaccurate when using current methodologies and theory. In this work, we circumvent the need to focus on detailed reconstructions of the concentration field by focusing on the geophysical response to the product of a mixing-driven reaction. By considering reactions whose products have significantly different electrical conductivity than the reactants, we suggest that this new strategy potentially offers enhanced sensitivity to mixing processes. This approach is akin to the "smart tracer" methodology proposed by Haggerty et al. (2008), who developed a reactive tracer changing color when exposed to aerobic respiration, thus allowing quantification of biogeochemical processes in transient storage zones of stream ecosystems (Haggerty et al., 2009; Liao & Cirpka, 2011). Here to image reactive mixing processes in the subsurface we propose a smart tracer that produces an electrically sensitive solution when undergoing a mixing-driven reaction.

Many chemical reactions are limited by the mixing of initially segregated chemical species, which react upon mixing (De Simoni et al., 2005; Dentz et al., 2011; Le Borgne et al., 2014); these reactions include a large number of redox reactions, as well as precipitation reactions (Appelo & Postma, 2004). Mixing-limited reactions have been used to quantify mixing rates in laboratory experiments and through numerical simulations (Cirpka et al., 2006; de Anna, Dentz, et al., 2014; de Anna, Jimenez-Martinez, et al., 2014; Gramling et al., 2002; Rolle et al., 2009). Herein, we focus on mixing-limited reactions whose products have an electrical conductivity that is significantly different from that of the initial reactants. An example of such reactions is the oxidation of organic matter (see supporting information). While dissolved organic matter has a low electrical conductivity, the oxidation reaction releases dissolved anions with a much larger electrical conductivity. Other examples of reactions that could be explored are given in the supporting information.

We thus consider a configuration in which reactive mixing takes place at the interface of two miscible fluids, one displacing the other. We compute the spatial distribution of the product concentration and analyze its impact on the effective electrical conductivity (from here onward "conductivity" will always imply electrical conductivity, unless otherwise specified) produced by mixing fronts, as defined over the Darcy scale. Since molecular diffusion alone is comparatively inefficient at mixing fluids, mixing rates in groundwater systems are primarily dictated by the coupling of molecular diffusion and velocity gradients that elongate mixing fronts and enhance concentration gradients (Dentz et al., 2011; Le Borgne et al., 2014, 2013). As a proof of concept, we consider simple shear flows characterized by a range of velocity gradients that is representative of the deformation rates experienced by mixing fronts in heterogeneous porous media. The concentration fields of the reactive species are derived using the Lamellar Mixing Theory, a Lagrangian method that allows

for explicit analytical expressions relating front deformation to mixing and reaction rate (Bandopadhyay et al., 2017; Le Borgne et al., 2014; Meunier & Villermaux, 2010). The computed effective conductivity evolves in time under the combined effect of front stretching and of local changes in conductivity. The effective conductivity is observed to vary in time over several orders of magnitudes, as the reaction progresses. Our results further reveal that depending on the orientation of the applied electrical potential gradient with respect to the flow direction and shear plane, the effective conductivity is either more sensitive to the local stretching rate or to the reaction kinetics.

2. Reactive Mixing Fronts Generating Electrically Conductive Products

We investigate the electrical signature of reactive mixing in subsurface porous media by considering an irreversible reaction of the type

$$A + B \rightarrow C\,, \tag{1}$$

where A and B are two reactive species undergoing chemical transformation to produce C, which may be composed of ions D^+ and E^-. The forward reaction is governed by the reaction kinetics $R = K\,c'_A\,c'_B$, where R is the rate of reaction, K is the reaction rate constant, and c'_i is the concentration of the ith species. We assume that the product has larger electrical mobility than the reactants A and B, thus enhancing the local electrical conductivity of the pore fluid as the reaction progresses. This enhancement of the effective conductivity of the porous media can then be monitored to track the progress of the reaction and hence the dynamics of the mixing front. Some examples of reactions of the kind described by equation 1 that are of relevance to remediation and contaminant transport (Hort et al., 2014) are described in Table S1 of the supporting information. For simplicity, we assume that the two ionic products have the same electrical mobility v' (defined as the steady state velocity of an ion per unit force applied to it), while the background fluid conductivity of the subsurface media is given by σ'_b. The reacting species A and B are assumed to have the same molecular diffusion coefficient D_r. The diffusion coefficient of the product C is D_p. Finally, we assume that the pore fluid is electroneutral throughout the domain of interest.

Consider a mixing front where A displaces B in a heterogeneous porous medium (Figure 1), the mixing interface where species mix and react is deformed by velocity gradients induced by permeability fluctuations. The resulting elongation rates dictates the effective mixing and reaction rates (Le Borgne et al., 2014). At local scale, this process is analogous to the deformation created by a shear flow, which leads to a linear increase of the length of the mixing interface in time. As a proof of concept, we thus consider the paradigmatic simple shear flow scenario (Bandopadhyay et al., 2017). The presented methodology can be extended to heterogeneous permeability fields by considering nonlinear front elongations (Le Borgne et al., 2015) (see supporting information for further discussion). Initially, the two reactants are separated by a planar interface perpendicular to the flow direction. The externally imposed stationary flow is assumed two-dimensional, so that shear always occurs in the same plane (Figure 1). In this context, the coordinate system is defined as follows: the origin is placed at the center of the initial interface; the x axis is perpendicular to the front while the y axis is normal to the x axis but parallel to the plane of shear. The domain dimensions are $2L'_x$ and $2L'_y$ along the x and y axes. The front is initially at $x = 0$, and the velocity field given by $\mathbf{v}' = u'(y')\,\mathbf{e}_x$, where u' denotes the velocity profile and can be an arbitrary (but continuous) function of y', and $\mathbf{e}_x$ is the unit vector along the x axis. The local shear rate, generally defined as $\mathbf{\Gamma}'(\mathbf{x}') = \frac{1}{2}[\nabla\mathbf{v}' + (\nabla\mathbf{v}')^T]$, reduces to the form $\Gamma' = \mathrm{d}u'/\mathrm{d}y'$. While our theoretical description of reactive mixing (and its treatment through the Lamellar Mixing Theory, Le Borgne et al., 2014) concerns a general stratified flow, where the function u' varies across the front, all results presented in the following consider a simple shear flow. Indeed, any stratified flow can be decomposed into a superposition of different shear flows (see section S1.4 of the supporting information for further arguments in this respect). Shear deformation elongates the mixing front as

$$\rho = \sqrt{1 + (|\nabla\mathbf{v}'|t)^2}, \tag{2}$$

where ρ is the front elongation. This deformation process is characterized by the characteristic time $\tau_{sh} = |\nabla(\mathbf{v}')|^{-1}$ at which elongation starts growing linearly in time. It should be noted here that the superposition method described above applies only to the mass of product, while the exact nature of the electrical conductivity would depend on the extent of the domain and details of the spatial distributions of the conducting

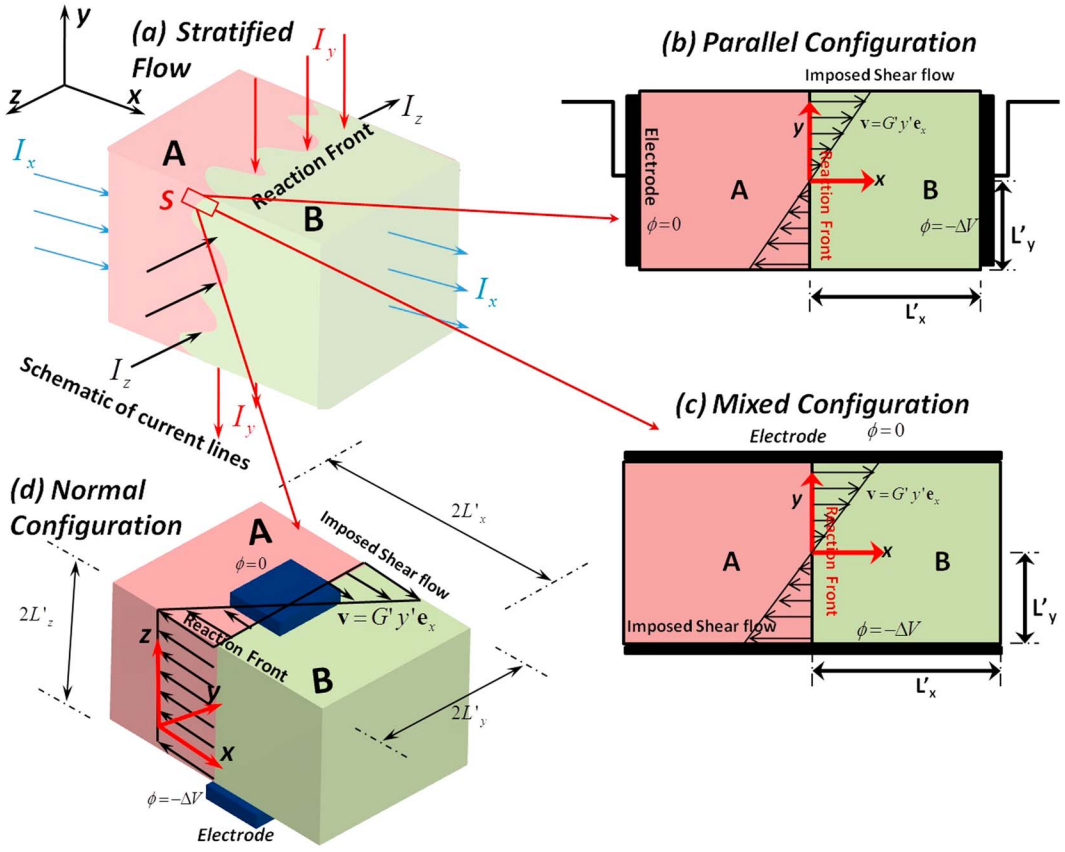

Figure 1. Schematic description of the system under consideration. (a) Stratified front between species A and B; the front can be constructed by superimposing individual shear flows, such as pictured in (b–d) magnified views (Figures 1b–1d). Based on the direction of the applied potential difference (or ΔV at the domain's scale) with respect to the shear flow, three exemplary configurations are distinguished: in the (b) *parallel configuration* ΔV is parallel to the flow direction; in the (c) *mixed configuration* ΔV is perpendicular to the flow direction but parallel to the plane of shear; in the (d) *normal configuration* ΔV is perpendicular to both the flow direction and the plane of shear. Note that in the normal configuration, the electrodes cover the full surface that is depicted; in order to avoid masking an important part of the sketch, only a small size electrode is shown.

species. However, through scaling arguments it can be shown that many important general features of the effective conductivity (see section 4 and the supporting information for more details), as evaluated based on a shear flow, remain valid for more complex flows.

To investigate the sensitivity of the effective electrical conductivity across the system under study to the reactive mixing dynamics, we assume that a uniform difference in electrical potential is applied across the domain of study, between two of its planar boundaries, opposite from each other. Depending on the relative orientations of this applied potential gradient ∇V, the flow and the plane of shear, three different configurations exist, which we refer to as the parallel, mixed, and normal configurations (Figures 1b–1d). In the parallel configuration, the flow and the applied potential gradient are parallel to each other. In the mixed configuration, ∇V is perpendicular to the flow but parallel to the plane of shear (Γ'_{xy}). In the normal configuration, ∇V is normal to the plane of shear and to the flow direction.

3. Mathematical Formulation

3.1. Governing Equations

The details of the dimensional equations are given in the supporting information. Here for the sake of brevity we directly introduce the nondimensional equations. The nondimensional version ξ of a dimensional variable ξ' is obtained as $\xi = \xi'/\xi_c$, where ξ_c is a characteristic value for this variable. As characteristic values, we choose the initial concentration of the reacting species, c'_0, for the concentration, the initial interface thickness, $x_c = w_0$, for the length scale, the potential difference applied across the domain, $\phi_c = \Delta V$, for the electrical

potential, $\sigma_c = e^2 v' c_0'$, (where e is the protonic charge), for the conductivity, $v_c = \Gamma_0 w_0$, (where Γ_0 is the mean shear rate), for the velocity and the diffusion time scale, $t_c = w_0^2/D_r$, where D_r is the reference diffusion coefficient of the reactants, for time. With the above description, the nondimensional equations take the following form:

$$\frac{\partial c_A}{\partial t} + Pe\mathbf{v}\cdot\boldsymbol{\nabla} c_A = \nabla^2 c_A - Da\left(c_A c_B\right), \tag{3}$$

$$\frac{\partial c_B}{\partial t} + Pe\mathbf{v}\cdot\boldsymbol{\nabla} c_B = \nabla^2 c_B - Da\left(c_A c_B\right), \tag{4}$$

$$\frac{\partial c_C}{\partial t} + Pe\mathbf{v}\cdot\boldsymbol{\nabla} c_C = \bar{D}\nabla^2 c_C + Da\left(c_A c_B\right), \tag{5}$$

$$\boldsymbol{\nabla}\cdot(\sigma\boldsymbol{\nabla}\phi) = 0. \tag{6}$$

In (6), the conductivity is given by $\sigma = F^{-1}\left(\sigma_r + 2c_D\right)$, where the nondimensional background fluid conductivity is $\sigma_r = \sigma_b'/\sigma_c$, σ_b' being the background conductivity of the medium. F is the formation factor (Archie, 1942) defined as $F = \varphi^{-m}$, φ being the porosity and m the cementation exponent related to the connectivity of the pore space. The velocity now has the expression, $\mathbf{v} = \Gamma(y)\,\mathbf{e}_x$. In equations (3)–(6), the nondimensional numbers are the Péclet number $Pe = v_c w_0/D_r$ and the Damköhler number $Da = Kc_0' w_0^2/D_r$. In this nondimensional formulation, the characteristic shear time is Pe^{-1} and the characteristic reaction time is Da^{-1}.

Equations (3)–(5) describe the transport of the reacting species and the product, while equation (6) governs the evolution of the electrical potential across the domain. Although the production of ions can change the local conductivities in several ways, here we assume that they only alter the pore fluid conductivity. As a result, the local electrical conductivity is described as a linear function of the local concentration. Therefore, the final equation governing electrical potential emerges from the conservation of current, given by $\mathbf{i} = -\sigma\boldsymbol{\nabla}\phi$. However, one should keep in mind that such a linear relation is only an approximate estimate, valid for dilute solutions. A more detailed discussion on this topic is included in the supporting information. Note that there is a one-way coupling between the species transport equations and the electrical potential in the domain and hence once the concentration of the ionic products are known, we can solve the current conservation equation i.e., equation (6) to evaluate the current and the resulting effective conductivity at the domain scale. The boundary conditions for the species concentration are as follows:

$$c_A = 1,\ c_B = 0,\ \text{at } x \to -\infty, \tag{7}$$

$$c_A = 0,\ c_B = 1,\ \text{at } x \to \infty, \tag{8}$$

$$c_C = 0 \text{ at } x \to \infty \text{ and } -\infty. \tag{9}$$

The initial conditions for the species concentration are given by

$$\text{At } t = 0,\ c_A = 1\ \forall\ x < 0 \text{ and } c_A = 0\ \forall\ x > 0, \tag{10}$$

$$c_B = 0\ \forall\ x < 0 \text{ and } c_B = 1\ \forall\ x > 0, \tag{11}$$

$$c_C = 0\ \forall\ x. \tag{12}$$

Finally, the boundary conditions for the electrical potential read as

$$\text{Parrallel Configuration: } \phi(0,y) = 0;\ \ \phi(L_x,0) = -1;\ \text{At } y = \pm L_y,\ \frac{\partial\phi}{\partial y} = 0; \tag{13}$$

$$\text{Mixed Configuration: } \phi(x,L_y) = -1;\ \phi(x,-L_y) = 0;\ \text{At } x = \pm L_x,\ \frac{\partial\phi}{\partial x} = 0; \text{and} \tag{14}$$

$$\text{Normal Configuration: } z = -L_z,\ \phi = -1;\ \ \text{At } z = L_z,\ \phi = 0. \tag{15}$$

The resulting nondimensional effective conductivity is evaluated from

$$\sigma_{\text{eff},k} = \frac{A_{\text{el},k}}{L_k I_{\text{el},k}};\ \text{where } I_{\text{el},k} = \int_{\text{electrode}} -\sigma\boldsymbol{\nabla}\phi\cdot\mathbf{n}_k \mathrm{d}S, \tag{16}$$

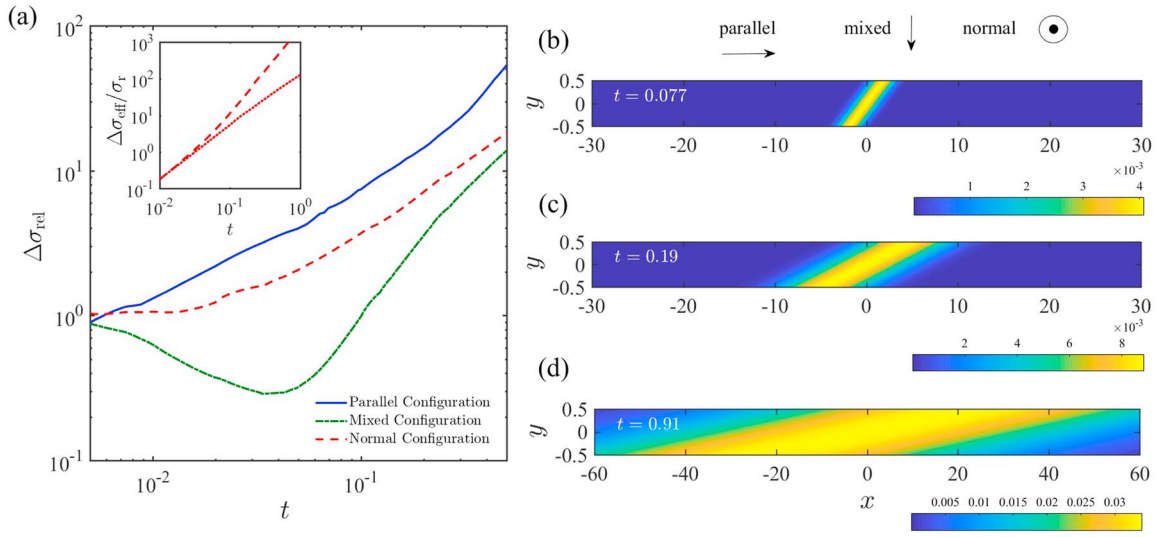

Figure 2. (a) Evolution of the relative change in effective conductivity ($\Delta\sigma_{rel}$, defined in equation (17) with time, for the three configurations and for $Pe = 50$ and $Da = 1$. We emphasize that we have taken the numerator of $\Delta\sigma_{rel}$ (i.e., $\Delta\sigma_{eff}$) for $Pe = 50$. The inset shows the evolution of $\Delta\sigma_{eff}$ normalized by the background conductivity σ_r for $Pe = 50$ (dotted line) and $Pe = 0$ (solid line), in the normal configuration. (b–d) Spatial distribution of product concentration (normalized by the initial reactant concentration) at nondimensional times (b) $t = 0.08$, (c) $t = 0.19$, and (d) $t = 0.91$; only fractions of the x axis, centered around the front, are shown.

where $k = 1$ denotes the parallel configuration, $k = 2$ the mixed configuration, and $k = 3$ the normal configuration; $A_{el,k}$ is the area of the electrode receiving the current; $I_{el,k}$ is the total current through the cross section of the electrode; and $\mathbf{n}_k$ is the unit vector normal to the electrode surface in the kth configuration. For instance, in the parallel configuration, we can write $A_{el} = 2L_y$, $L_1 = 2L_x$, and $\mathbf{n} = \mathbf{e}_x$. The above expression evaluates the total current at the electrode with the lower potential (i.e., the one that receives the current) and computes the effective conductivity (σ_{eff}) as the ratio of the applied potential difference to this current.

The governing equations for species transport are solved using the Lamella Mixing Theory (Le Borgne et al., 2014), while the equation for the electrical potential is solved numerically with a finite difference scheme. The detailed solution procedure for the species transport equations is given in section 2 of the supporting information. Finally, note that for the normal configuration (see Figure 1d), it is possible to find semianalytical solutions for σ_{eff} (see section 2.3 in the supporting information), showing that σ_{eff} in this configuration is linearly proportional to the mass of the product.

4. Results and Discussions

From solving the equations above, we investigate the signature of reactive mixing on the effective conductivity σ_{eff} for a shear flow at arbitrary Péclet numbers Pe and Damköhler numbers Da. The domain's dimensionless sizes are $L_x = 300$ and $L_y = 0.5$. This large aspect ratio was chosen to ensure that the reaction front does not reach the end of the domain of choice during the investigated time. The chosen values of the dimensionless parameters are $\sigma_r = 10^{-5}$, $\bar{D} = 1$, and $\varphi = 0.4$. Possible values of the quantity σ_r, tabulated in Table 1 of the supporting information for various reactions of the type given by equation (1) show that σ_r varies between 10^{-1} and 10^{-7} in natural systems. In addition to this, the probable ranges for the Damköhler number Da are specified for some selected reactions in Table S2 of the supporting information. As a signature of reactive mixing, we analyze the temporal evolution of the net change in effective conductivity, defined as $\Delta\sigma_{eff} = \sigma_{eff} - \sigma_r$.

The product concentration field is shown in Figures 2b–2d at three different times for $Pe = 50$ and $Da = 1$. Reactive mixing at the interface of the two reactants creates a highly conducting zone in the central part of the domain, surrounded by two regions of low conductivity. This band broadens as the reaction progresses. This induces a significant increase in σ_{eff}, which can be 3 orders of magnitude larger than the background (see inset of Figure 2a). Under shear flow, the evolution of effective conductivity deviates from the $Pe = 0$ case, as velocity gradients strongly impact the mixing dynamics and thus the spatial distribution of the product of reaction (Figures 2b–2d).

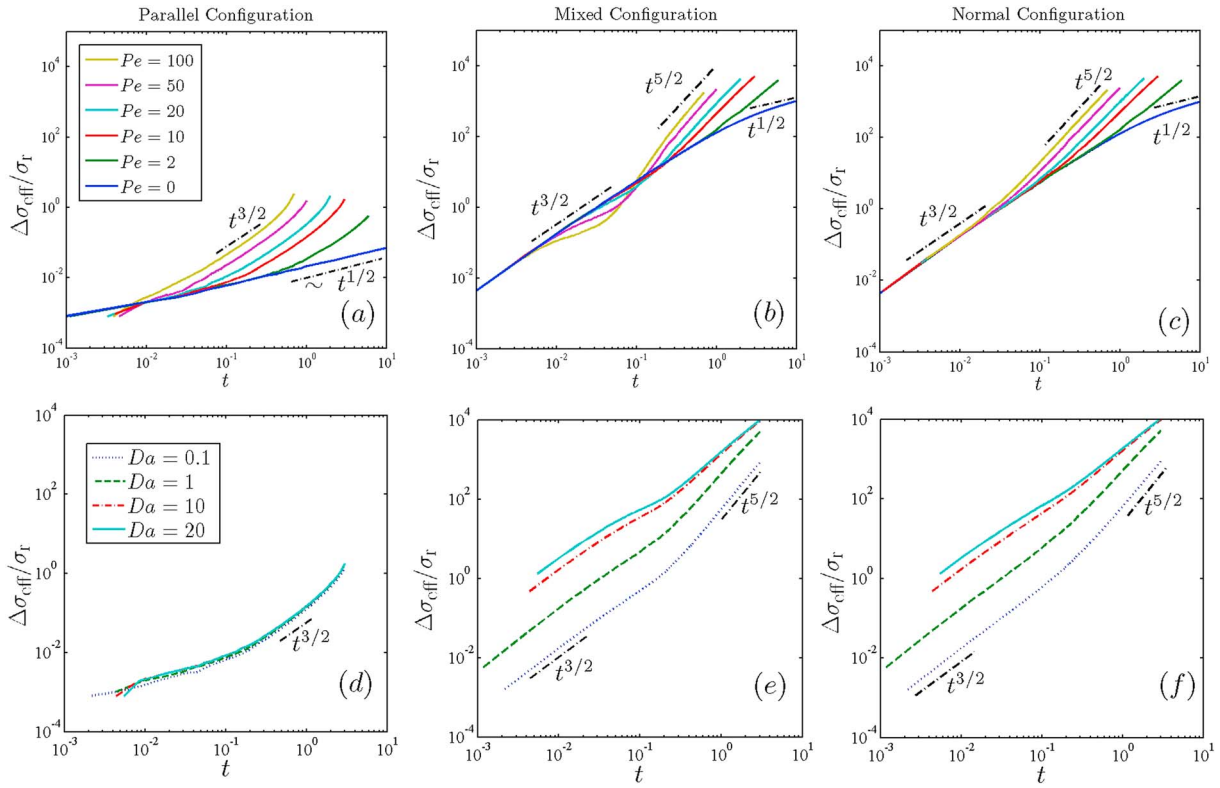

Figure 3. Evolution of the normalized $\Delta\sigma_{\mathrm{eff}}$ with $t = t'/t_{\mathrm{c}}$ in the three configurations: (a and d) parallel configuration, (b and e) mixed configuration, and (c and f) normal configuration. In Figures 3a–3c, evolutions of $\Delta\sigma_{\mathrm{eff}}$ are shown for different Péclet numbers (Pe), for $Da = 1$. In Figures 3d–3f the evolutions in $\Delta\sigma_{\mathrm{eff}}$ are showcased for different Damköhler numbers (Da), for $Pe = 10$. Dash-dotted lines indicate theoretical scaling laws.

To compare the sensitivity of the different configurations to the flow heterogeneity, we normalize the effective conductivity by the effective conductivity in the absence of shear as

$$\Delta\sigma_{\mathrm{rel}} = \frac{\sigma_{\mathrm{eff}} - \sigma_{\mathrm{r}}}{\left(\sigma_{\mathrm{eff}} - \sigma_{\mathrm{r}}\right)_{Pe=0}}. \tag{17}$$

The results show that the parallel configuration is the most sensitive to the effects of stretching (Figure 2a). Furthermore, while $\Delta\sigma_{\mathrm{rel}}$ monotonically increases for the parallel and normal configurations (Figure 1d), for the mixed configuration (Figure 1c) it first decreases and then rapidly increases with time by several orders of magnitude. Such distinct behaviors between the different configurations can be explained by considering the spatial distribution of the product at different times (Figures 2b–2d). In the Parallel Configuration, the regions of low and high conductivity are approximately in series, while for the other two configurations they can be thought to be approximately acting in parallel, at least at early times. Therefore, σ_{eff} in the parallel configuration shows more sensitivity to the width of this highly conducting zone. Since the stretching of the reaction front speeds up the reaction rate as well as increases the width of the front, it creates a larger impact on σ_{eff} when measured in this configuration. In addition, since σ_{eff} in the normal configuration is linearly proportional to the mass of the product, it increases monotonically with time like the mass of product. Finally, σ_{eff} in the mixed configuration is slightly more complicated. The initial drop in $\Delta\sigma_{\mathrm{eff}}$ for this configuration can be explained by considering the path of least resistance for the current. In this configuration most of the current flows through the highly conducting band in the reaction front. Because of the nature of the flow, this front is stretched along its length, which also stretches the path of least resistance for the current. This naturally leads to an increased resistance to the current at early times, which results in a decrease in $\Delta\sigma_{\mathrm{rel}}$. However, as the reaction progresses, this trend is reversed because of a significant increase in the local conductivity, due to the increase in the mass of the ions and the width of the front. Therefore, to summarize, the drop in $\Delta\sigma_{\mathrm{eff}}/\Delta\sigma_{\mathrm{eff},Pe=0}$ is the result of the changing orientation of the front, driven by stretching. In cases where diffusion-driven dispersion/widening is dominant, this drop in $\Delta\sigma_{\mathrm{eff}}$ is negligible (see Figure 3b).

To test the sensitivity of this idealized geoelectric response to the flow heterogeneity, the mixing rate, and the reaction kinetics, we analyze the effect of varying the Péclet and Damköhler numbers. Results are shown in Figures 3a–3c for $Da = 1$ and various Pe, and in Figures 3d–3f for $Pe = 10$ and various Da. We first concentrate on Figures 3a–3c. For all cases, the effective electrical conductivity initially follows the trend observed in the absence of velocity gradients ($Pe = 0$). As the effect of shear becomes predominant, the curves deviate, showing the sensitivity of the geoelectric response to enhanced mixing due to shear. Larger values of Pe result in earlier deviations from the $Pe = 0$ case, as quantified by the shear time Pe^{-1}. The observed trends are otherwise similar to those described in Figure 2. Figures 3d–3f show the sensitivity of the different configurations to the reaction kinetics. We note that the mixed and the normal configurations are far more sensitive to changes in the reaction constant K (i.e., increase in Da) as compared to the parallel configuration, which shows almost no sensitivity to the reaction rate. From the orientation of the front in the different configurations (Figure 2b–2d), we infer that in the parallel configuration, $\Delta\sigma_{\text{eff}}$ is more sensitive to the width of the zone of high conductivity, since the regions of low and higher conductivity are approximately in series here. This is in contrast to the other two configurations for which these regions are approximately in parallel. Because the width of the zone of higher conductivity is strongly dictated by Pe, the parallel configuration is naturally more sensitive to changes in Pe. Since Da does not influence the width of the reaction front, the parallel configuration does not show much sensitivity to Da. We further infer that for the other two configurations, $\Delta\sigma_{\text{eff}}$ is sensitive to the total mass of the product, which is directly linked to reaction kinetics.

We complement the above results with scaling estimates of σ_{eff}. The details of the scaling derivation is given in the supporting information. In the parallel configuration, the asymptotic scaling of the effective conductivity is approximately $\Delta\sigma_{\text{eff}} \sim \sigma_r w(t)/L_x$, where $w(t)$ is the width of the highly conducting zone in the direction parallel to the mean current. Before the shear time $t < Pe^{-1}$, the front of reaction is not significantly tilted by shear and its width grows diffusively $w(t) \sim t^{1/2}$, which leads to $\Delta\sigma_{\text{eff}} \sim t^{1/2}$. After the shear time, shear enhances the growth of the projected width such that $w(t) \sim t^{3/2}$ and hence $\Delta\sigma_{\text{eff}} \sim t^{3/2}$. These approximate scaling laws are confirmed in Figure 3(a). This scaling pattern also helps to explain why $\Delta\sigma_{\text{eff}}$ depends very weakly on Da, since Da does not appear anywhere in the above expressions. In contrast, for the normal and mixed configurations the effective electrical conductivity is approximately $\Delta\sigma_{\text{eff}} \sim m_c(t)/L_x$, where $m_c(t)$ is the mass of the product per unit length of the front. The scaling laws of the mass of product in a reactive front submitted to shear flow have been derived by Bandopadhyay et al. (2017). For $t < Pe^{-1}$, the effect of shear is negligible and the mass of product is expected to evolve as $m_c(t) \sim Dat^{3/2}$ in the reaction kinetics limited regime ($t < Da^{-1}$) and $m_c(t) \sim t^{1/2}$ in the diffusion limited regime ($t > Da^{-1}$, weak stretching scenario, $Da > Pe$). For $t > Pe^{-1}$, shear enhances the mixing rate and the mass of product is expected to evolve as $m_c(t) \sim PeDat^{5/2}$ (for strong stretching, $Pe > Da$) in the reaction kinetics limited regime ($t < Da^{-1}$) and $m_c(t) \sim Pet^{3/2}$ in the diffusion limited regime ($t > Da^{-1}$). These scaling laws (particularly the ones related to strong stretching) explain the tendencies observed in Figures 3c and 3f for the normal configuration. In the mixed configuration, the trends are similar although there is a departure from the $t^{3/2}$ scaling law at short to intermediate times in Figure 3b due to the tilted orientation of the front, as discussed above.

5. Conclusions

Our results reveal several important aspects regarding the geoelectrical signatures of idealized reactive mixing and provide new insights on the possible development of smart geophysical tracers sensitive to mixing processes. First, the production of ions significantly changes the effective conductivity of the subsurface over time for all considered configurations. In the highly idealized system considered herein in which we ignore the presence of any other ions than the reactants and products of the reactions, we observe changes of several (up to 3) orders of magnitude. The net change in effective conductivity is more pronounced for what we refer to as the mixed and normal configurations. Our analysis shows that the different configurations may provide insights into different aspects of subsurface reactive mixing. Indeed, while the parallel configuration exhibits a high sensitivity to shear rate and, consequently, to the strength of the flow (as denoted by Pe), as well as to the width of the reaction front, the two other configurations are more sensitive to the reaction kinetics, controlled by the Damköhler number Da. Assuming the sensitivity of experimental measurements to be $\sim 1\%$ (Jougnot et al., 2016), our results reveal that in all three configurations, the changes in the effective conductivity from the reactions should be detectable. As a note of caution, further discussions on the possible consequences of some of the assumptions undertaken herein along with suggestions for potential laboratory experiments to test the method proposed herein are discussed in section S4 of the supporting information. Finally, we note

that the general conclusions of the present analysis (for instance, on the sensitivity of the various configurations) could be extended to heterogeneous hydraulic conductivity fields as well, since differences in hydraulic conductivity produce velocity gradients that deform mixing fronts in a way similar to shear (Le Borgne et al., 2015). This is confirmed by preliminary results obtained for heterogeneous Darcy flows.

In essence, the present theoretical/numerical analysis suggests that monitoring of the effective electrical conductivity of a region of the subsurface may provide quantitative information on mixing and reactions. One does not always have a priori knowledge of the geometric configuration of subsurface flows, so electrical conductivity measurements with different orientations of the sensor arrays could allow inferring the flow orientation as well as estimates of stretching rates and reaction rates, for certain kinds of reactions. In addition, this study shows that, in the presence of shear flow, the electrical conductivity resulting from reactive mixing is by nature anisotropic and should be considered a tensor. The scope of the present study can be expanded by including the effects of the electrical double layers around the grain surfaces, which would enhance the effective conductivity and play a major role in low permeability media. Another prospect is the further development of the present method to investigate the complex conductivity or spectral induced polarization response (Leroy et al., 2017; Maineult et al., 2017; Okay et al., 2014) of a similar reactive mixing phenomenon, in an effort to extract additional information allowing to better monitor reactive mixing in the subsurface.

Acknowledgments
We gladly acknowledge fruitful discussions with Khalil Hanna on redox reactions. U. G., Y. M., and T. L. B. gratefully acknowledge the financial support from the European Commission's Marie Sklodowska-Curie Actions through the project "GeoElectricMixing" along with financial support from the European Research Council (ERC) through the project "ReactiveFronts" (648377). This is a theoretical paper. Since we have not performed any experiments, there is no data to report. All the results of the theoretical and numerical analysis have been shown in the plots. Any data taken from any other sources have been provided with proper references.

References

Appelo, C. A. J., & Postma, D. (2004). *Geochemistry, groundwater and pollution*. Amsterdam, NL: CRC press.

Archie, G. E. (1942). The electrical resistivity log as an aid in determining some reservoir characteristics. *Transactions of the AIME*, *146*(01), 54–62.

Atekwana, E. A., & Slater, L. D. (2009). Biogeophysics: A new frontier in Earth science research. *Reviews of Geophysics*, *47*, RG4004. https://doi.org/10.1029/2009RG000285

Bandopadhyay, A., Le Borgne, T., Méheust, Y., & Dentz, M. (2017). Enhanced reaction kinetics and reactive mixing scale dynamics in mixing fronts under shear flow for arbitrary Damköhler numbers. *Advances in Water Resources*, *100*, 78–95.

Binley, A., Cassiani, G., Middleton, R., & Winship, P. (2002). Vadose zone flow model parameterisation using cross-borehole radar and resistivity imaging. *Journal of Hydrology*, *267*(3), 147–159.

Binley, A., Hubbard, S. S., Huisman, J. A., Revil, A., Robinson, D. A., Singha, K., & Slater, L. D. (2015). The emergence of hydrogeophysics for improved understanding of subsurface processes over multiple scales. *Water Resources Research*, *51*, 3837–3866. https://doi.org/10.1002/2015WR017016

Boano, F., Harvey, J. W., Marion, A., Packman, A. I., Revelli, R., Ridolfi, L., & Wörman, A. (2014). Hyporheic flow and transport processes: Mechanisms, models, and biogeochemical implications. *Reviews of Geophysics*, *52*, 603–679. https://doi.org/10.1002/2012RG000417

Briggs, M. A., Day-Lewis, F. D., Ong, J. B., Curtis, G. P., & Lane, J. W. (2013). Simultaneous estimation of local-scale and flow path-scale dual-domain mass transfer parameters using geoelectrical monitoring. *Water Resources Research*, *49*, 5615–5630. https://doi.org/10.1002/wrcr.20397

Briggs, M. A., Day-Lewis, F. D., Ong, J. B., Harvey, J. W., & Lane, J. W. (2014). Dual-domain mass-transfer parameters from electrical hysteresis: Theory and analytical approach applied to laboratory, synthetic streambed, and groundwater experiments. *Water Resources Research*, *50*, 8281–8299. https://doi.org/10.1002/2014WR015880

Cassiani, G., Bruno, V., Villa, A., Fusi, N., & Binley, A. M. (2006). A saline trace test monitored via time-lapse surface electrical resistivity tomography. *Journal of Applied Geophysics*, *59*(3), 244–259.

Chiogna, G., Hochstetler, D., Bellin, A., Kitanidis, P., & Rolle, M. (2012). Mixing, entropy and reactive solute transport. *Geophysical Research Letters*, *39*, L20405. https://doi.org/10.1029/2012GL053295

Cil, M. B., Xie, M., Packman, A. I., & Buscarnera, G. (2017). Solute mixing regulates heterogeneity of mineral precipitation in porous media. *Geophysical Research Letters*, *44*, 6658–6666. https://doi.org/10.1002/2017GL073999

Cirpka, O. A., & Kitanidis, P. K. (2000). Characterization of mixing and dilution in heterogeneous aquifers by means of local temporal moments. *Water Resources Research*, *36*(5), 1221–1236. https://doi.org/10.1029/1999WR900354

Cirpka, O. A., Olsson, A., Ju, Q. S., Rahman, M. A., & Grathwohl, P. (2006). Determination of transverse dispersion coefficients from reactive plume lengths. *Ground Water*, *44*, 212–221.

Cirpka, O. A., Schwede, R. L., Luo, J., & Dentz, M. (2008). Concentration statistics for mixing-controlled reactive transport in random heterogeneous media. *Journal of Contaminant Hydrology*, *98*, 61–74.

Daily, W., Ramirez, A., LaBrecque, D., & Nitao, J. (1992). Electrical resistivity tomography of vadose water movement. *Water Resources Research*, *28*(5), 1429–1442.

Day-Lewis, F. D., Linde, N., Haggerty, R., Singha, K., & Briggs, M. A. (2017). Pore-network modeling of the electrical signature of solute transport in dual-domain media. *Geophysical Research Letters*, *44*, 4908–4916. https://doi.org/10.1002/2017GL073326

de Anna, P., Dentz, M., Tartakovsky, A., & Le Borgne, T. (2014). The filamentary structure of mixing fronts and its control on reaction kinetics in porous media flows. *Geophysical Research Letters*, *41*, 4586–4593. https://doi.org/10.1002/2014GL060068

de Anna, P., Jimenez-Martinez, J., Tabuteau, H., Turuban, R., Le Borgne, T., Derrien, M., & Meheust, Y. (2014). Mixing and reaction kinetics in porous media: An experimental pore scale quantification. *Environmental Science & Technology*, *48*(508-516), 508–516.

de Barros, F. P. J., Dentz, M., Koch, J., & Nowak, W. (2012). Flow topology and scalar mixing in spatially heterogeneous flow fields. *Geophysical Research Letters*, *39*, L08404. https://doi.org/10.1029/2012GL051302

De Simoni, M., Carrera, J., Sanchez-Vila, X., & Guadagnini, A. (2005). A procedure for the solution of multicomponent reactive transport problems. *Water Resources Research*, *41*, W11410. https://doi.org/10.1029/2005WR004056

Dentz, M., Le Borgne, T., Englert, A., & Bijeljic, B. (2011). Mixing, spreading and reaction in heterogeneous media: A brief review. *Journal of Contaminant Hydrology*, *120*, 1–17.

Doetsch, J., Linde, N., Vogt, T., Binley, A., & Green, A. G. (2012). Imaging and quantifying salt-tracer transport in a riparian groundwater system by means of 3D ERT monitoring. *Geophysics*, *77*(5), B207–B218.

Dorn, C., Linde, N., Le Borgne, T., Bour, O., & Baron, L. (2011). Single-hole GPR reflection imaging of solute transport in a granitic aquifer. *Geophysical Research Letters*, *38*, L08401. https://doi.org/10.1029/2011GL047152

Engdahl, N. B., Benson, D. A., & Bolster, D. (2014). Predicting the enhancement of mixing-driven reactions in nonuniform flows using measures of flow topology. *Physical Review E*, *90*(5), 051001.

Gramling, C. M., Harvey, C. F., & Meigs, L. C. (2002). Reactive transport in porous media: A comparison of model prediction with laboratory visualization. *Environmental Science & Technology*, *36*, 2508–2514.

Haggerty, R., Argerich, A., & Martí, E. (2008). Development of a "smart" tracer for the assessment of microbiological activity and sediment-water interaction in natural waters: The resazurin-resorufin system. *Water Resources Research*, *44*, W00D01. https://doi.org/10.1029/2007WR006670

Haggerty, R., Martí, E., Argerich, A., von Schiller, D., & Grimm, N. B. (2009). Resazurin as a "smart" tracer for quantifying metabolically active transient storage in stream ecosystems. *Journal of Geophysical Research*, *114*, G03014. https://doi.org/10.1029/2008JG000942

Hidalgo, J. J., Dentz, M., Cabeza, Y., & Carrera, J. (2015). Dissolution patterns and mixing dynamics in unstable reactive flow. *Geophysical Research Letters*, *42*, 6357–6364. https://doi.org/10.1002/2015GL065036

Hort, R. D., Revil, A., & Munakata-Marr, J. (2014). Analysis of sources of bulk conductivity change in saturated silica sand after unbuffered TCE oxidation by permanganate. *Journal of Contaminant Hydrology*, *165*, 11–23.

Hubbard, S., & Linde, N. (2011). Hydrogeophysics. In P. Wilderer (Ed.), *Treatise on water science* (Vol. 1, pp. 401–434). Oxford: Academic Press.

Jougnot, D., Jimenez-Martinez, J., Legendre, R., Le Borgne, T., Meheust, Y., & Linde, N. (2018). Impact of small-scale saline tracer heterogeneity on electrical resistivity monitoring under saturated and partially saturated conditions: Insights from geoelectrical milli-fluidic experiments. *Advances in Water Resources*, *113*, 295–309. https://doi.org/10.1016/j.advwatres.2018.01.014

Jougnot, D., Jiménez-Martínez, J., Méheust, Y., Le Borgne, T., & Linde, N. (2016). Electrical resistivity monitoring of saline tracer fingering at pore scale under partially saturated conditions. In *Near Surface Geoscience 2016-22nd European Meeting of Environmental and Engineering Geophysics*. Barcelona, Spain.

Kemna, A., Binley, A., Cassiani, G., Niederleithinger, E., Revil, A., Slater, L., et al. (2012). An overview of the spectral induced polarization method for near-surface applications. *Near Surface Geophysics*, *10*(6), 453–468.

Kitanidis, P. K (1994). The concept of the dilution index. *Water Resources Research*, *30*, 2011–2026.

Kitanidis, P. K., & McCarty, P. L. (2012). *Delivery and mixing in the subsurface: Processes and design principles for in situ remediation* (Vol. 4). New York: Springer Science & Business Media.

Knight, R., Pyrak-Nolte, L. J., Slater, L., Atekwana, E., Endres, A., Geller, J., et al. (2010). Geophysics at the interface: Response of geophysical properties to solid-fluid, fluid-fluid, and solid-solid interfaces. *Reviews of Geophysics*, *48*, RG4002. https://doi.org/10.1029/2007RG000242

Le Borgne, T., Dentz, M., Bolster, D., Carrera, J., De Dreuzy, J.-R., & Davy, P. (2010). Non-Fickian mixing: Temporal evolution of the scalar dissipation rate in heterogeneous porous media. *Advances in Water Resources*, *33*(12), 1468–1475.

Le Borgne, T., Dentz, M., & Villermaux, E. (2013). Stretching, coalescence and mixing in porous media. *Physical Review Letters*, *110*, 204501.

Le Borgne, T., Ginn, T. R., & Dentz, M. (2014). Impact of fluid deformation on mixing-induced chemical reactions in heterogeneous flows. *Geophysical Research Letters*, *41*, 7898–7906. https://doi.org/10.1002/2014GL062038

Le Borgne, T., Dentz, M., & Villermaux, E. (2015). The lamellar description of mixing in porous media. *Journal of Fluid Mechanics*, *770*, 458–498.

Leroy, P., Li, S., Jougnot, D., Revil, A., & Wu, Y. (2017). Modelling the evolution of complex conductivity during calcite precipitation on glass beads. *Geophysical Journal International*, *209*(1), 123–140.

Lester, D. R., Metcalfe, G., & Trefry, M. G. (2013). Is chaotic advection inherent to porous media flow? *Physical Review Letters*, *111*, 174101.

Liao, Z., & Cirpka, O. A. (2011). Shape-free inference of hyporheic traveltime distributions from synthetic conservative and "smart" tracer tests in streams. *Water Resources Research*, *47*, W07510. https://doi.org/10.1029/2010WR009927

Luo, J., Dentz, M., Carrera, J., & Kitanidis, P. (2008). Effective reaction parameters for mixing controlled reactions in heterogeneous media. *Water Resources Research*, *44*, W02416. https://doi.org/10.1029/2006WR005658

Maineult, A., Revil, A., Camerlynck, C., Florsch, N., & Titov, K. (2017). Upscaling of spectral induced polarization response using random tube networks. *Geophysical Journal International*, *209*(2), 948–960.

McClain, M. E., Boyer, E. W., Dent, C. L., Gergel, S. E., Grimm, N. B., & Groffman, P. M. (2003). Biogeochemical hot spots and hot moments at the interface of terrestrial and aquatic ecosystems. *Ecosystems*, *6*, 301–312.

Meunier, P., & Villermaux, E. (2010). The diffusive strip method for scalar mixing in two dimensions. *Journal of Fluid Mechanics*, *662*, 134–172.

Okay, G., Leroy, P., Ghorbani, A., Cosenza, P., Camerlynck, C., Cabrera, J., et al. (2014). Spectral induced polarization of clay-sand mixtures: Experiments and modeling. *Geophysics*, *79*(6), E353–E375.

Possemiers, M., Huysmans, M., Anibas, C., Batelaan, O., & Van Steenwinkel, J. (2016). Reactive transport modeling of redox processes to assess fe (OH)3 precipitation around aquifer thermal energy storage wells in phreatic aquifers. *Environmental Earth Sciences*, *75*(8), 648–664.

Rolle, M., Eberhardt, C., Chiogna, G., Cirpka, O. A., & Grathwohl, P. (2009). Enhancement of dilution and transverse reactive mixing in porous media: Experiments and model-based interpretation. *Journal of Contaminant Hydrology*, *110*(3), 130–142.

Singha, K., & Gorelick, S. M. (2005). Saline tracer visualized with three-dimensional electrical resistivity tomography: Field-scale spatial moment analysis. *Water Resources Research*, *41*, W05023. https://doi.org/10.1029/2004WR003460

Ye, Y., Chiogna, G., Cirpka, O. A., Grathwohl, P., & Rolle, M. (2015). Experimental evidence of helical flow in porous media. *Physical Review Letters*, *115*, 194502.